Transmission of Force and Displacement within the Myosin Molecule†

Takashi Ohki,‡ Sergey V. Mikhailenko,‡ Manuel F. Morales,§ Hirofumi Onishi,*,‡ and Naoki Mochizuki‡

Department of Structural Analysis, National Cardiovascular Center Research Institute, Fujishiro-dai, Suita, Osaka 565-8565, Japan, and University of the Pacific, San Francisco, California 94115

Received May 23, 2004; Revised Manuscript Received August 14, 2004

ABSTRACT: Myosin is a repetitive impeller of actin, using its catalysis of ATP hydrolysis to derive repeatedly the required free energy decrements. In each impulsion, changes at the myosin active site are transmitted through a series of structural elements to the myosin propeller (lever arm), almost 5 nm away. While the nature of transmission through most elements is evident, that through the so-called converter is not. To investigate how the converter changes linear displacement into rotation, we tested (one at a time) the effect of two Phe residue mutations (at 721 and 775) in the converter on the overall function of a heavy meromyosin (or subfragment 1) system, after first showing by observing kinetic behaviors that neither mutation affects other elements in the transmission. Using three tests (direct movement of the lever arm, activity in a motility assay with actin filaments, and direct force measurement of lever arm function), we found that these mutations affected only movements of the converter and the lever arm. From interpreting our observations in terms of the structure of the converter, we deduce that the linear−rotational transformation in the converter is mediated by a little machine (two Phe residues linked to a Gly) within a machine.

Myosin is the enzyme that catalyzes the hydrolysis of ATP, liberating the free energy used for the actin-propelling work in muscle contraction (*1*, *2*). But now, at the scale that can be accessed by X-ray crystallography and electron microscopy, myosin is seen as a complicated machine of many moving parts (*3*−*9*). Its catalytic function (conducted at its active site) is a long distance from the site of its actin propeller (lever arm) (*5*, *6*). Intervening are the relay helix and a poorly understood structure called the converter (*7*, *8*). When hydrolysis at the active site is transduced into force and displacement, these effects are transmitted by the intervening elements to the lever arm (*7*, *8*). Our aim is to understand how the overall transmission is accomplished, so we have to determine how the converter works. To get at this, we alter the converter structure by two especially chosen site-directed mutations, and draw inferences from what we observe. However, what we observe (changes in the movement of the lever arm resulting from a mutation) is meaningful only if we are sure that the mutation alters the converter element alone. Logically, we must begin with evidence that this is true.

The chemical kinetics describing the changes undergone by a myosin system are aptly described by the differential equation of Bagshaw and Trentham (B−T) (*10*, *11*). The equation tracks in time, *t*, the linear succession of the predominant myosin species, $M_i(t)$, as the enzyme binds the substrate and changes conformation, etc., and later as it sheds first the inorganic phosphate (P_i) and then ADP. Elsewhere, we (*12*, *13*) and others (*14*, *15*) show why the early stages in this succession report transformations at, or near, the active site, and then remote effects on the relay helix. Toward the end of ATP degradation, the stages report the $M_i(t)$ during the release of products, P_i and ADP. Once the numerical values of the rate constants of the equation are known, the equation allows the complete simulation of the degradation, or, if one wishes, of its early and late phases.

With this prospect in mind, three heavy meromyosin (HMM)[1] systems are prepared. One is normal (wild-type) HMM, and the others are the special mutants, in which Phe residues at positions 721 and 775 are replaced with Ala (F721A and F775A, respectively). It is known that both altered positions are located within the converter (*7*). With each system, standard experiments are performed to obtain the matrix of B−T rate constants, wherein some constants alone describe the early and some the late stages of ATP degradation. By comparing the kinetic data from the wild-type and mutant systems, we find that these particular mutations do not matter in the early events involving the active site or the relay helix, and also that they do not matter in the late events of ATP degradation. These findings warrant the conclusion that when performance tests of transmission detect any differences upon mutation, the differences are, most likely, effects on the converter, not adventitious effects on other elements of the system. Next, using three performance tests of transmission, we show that the test scores

† Supported by grants from the Ministry of Education, Culture, Sports, Science and Technology (to H.O. and N.M.), from the Ministry of Health, Labour and Welfare (to N.M.), and from the National Science Foundation (to M.F.M.).

* To whom correspondence should be addressed. Telephone: +81-6-6833-5012. Fax: +81-6-6872-8092. E-mail: honishi@ri.ncvc.go.jp.

‡ National Cardiovascular Center Research Institute.

§ University of the Pacific.

[1] Abbreviations: HMM, heavy meromyosin; S1, subfragment 1; mant-ATP, 2′(3′)-*O*-(*N*-methylanthraniloyl)adenosine 5′-triphosphate; RLC, regulatory light chain; ELC, essential light chain; CFP, cyan fluorescent protein; YFP, yellow fluorescent protein.

10.1021/bi048954f CCC: $27.50
Published on Web 10/09/2004

differ greatly in the middle phase involving the converter. After understanding the detailed structure of the converter, we work back by model building to understand how nucleotide binding, cleft closure, and subsequent events are connected with the converter, and thus, we obtain an overview of the transmission process (in the Discussion).

MATERIALS AND METHODS

Preparation of Recombinant HMMs and S1s. A chicken smooth-muscle myosin heavy chain cDNA clone was supplied by T. Masaki (*16*). A baculovirus transfer vector for wild-type HMM, with the His tag sequence at its N-terminal end and the myc tag sequence at its C-terminal end, in pFastBacHTa (Clontech, Palo Alto, CA), was produced as described previously (*17*). Site-directed mutagenesis was carried out using Kunkel's method (*18*) to replace Phe-721 or Phe-775 in the heavy chain sequence with alanine residues.

The cDNA for yellow fluorescent protein (YFP) was amplified from pEYFP-C1 (Clontech, Palo Alto, CA) by the polymerase chain reaction (PCR), creating an *Afl*III site at its N-terminus and an *Nco*I site at its C-terminus. The PCR product was digested with *Afl*III and *Nco*I, and subcloned into pFastBacHTa (named pFastBacHT-YFP). A transfer vector for the full-length sequence of the YFP-fused subfragment 1 (S1) heavy chain was prepared as described previously (*19*), but with pFastBacHT-YFP instead of pFastBacHTa.

The cDNA for cyan fluorescent protein (CFP) was amplified from pECFP-C1 (Clontech) by PCR with the same primers that were used in amplifying YFP. The PCR product was digested with *Afl*III and *Nco*I, and subcloned into pFastBacNN (*19*) (named pFastBacNN-CFP). pG17-1, which was plasmid pUC118 encoding the myosin essential light chain (ELC) and including a unique *Afl*III site at its initiating methionine codon (*20*), was digested with *Afl*III and *Pst*I, and subcloned into pFastBacNN-CFP. pRLCA, which was plasmid pUC119 encoding the myosin regulatory light chain (RLC) (*20*), was digested with *Afl*III and *Eco*RI, and subcloned into pFastBacNN. A *Bst*1107I site was created at the unique *Avr*II site of the transfer vector and was then digested with *Bst*1107I. To make a transfer vector for both myosin light chains, a cDNA fragment containing the coding region of the RLC was ligated into the *Bst*1107I site of the transfer vector containing the CFP-fused ELC sequence.

Expression and purification of wild-type and mutant HMMs were carried out as described previously (*17*). Chimeric S1s (named C/Y-S1), in which YFP was fused to the N-terminus of the S1 heavy chain and CFP was fused to the N-terminus of the ELC, were prepared by essentially the same method that was used for preparing recombinant S1s (*19*).

Stopped-Flow Experiments. Stopped-flow experiments were performed using an SF61-DX2 stopped-flow spectrophotometer (Hi-Tech Scientific, Salisbury, U.K.) with a 75 W Xe/Hg lamp, as described previously (*12*).

Fluorescence Measurements. Steady-state fluorescence was measured using an F-4500 fluorescence spectrophotometer (Hitachi, Tokyo, Japan). CFP (donor) was excited at 433 nm, and its emitted spectra were recorded from 450 to 600 nm. Efficiencies (E) were calculated from donor fluorescence quenching at 475 nm as $1 - F_{DA}/F_D$, where F_{DA} is the fluorescence of the C/Y-S1 and F_D is the fluorescence of S1 fused by CFP only. CFP and YFP were treated as point masses. The distance between CFP and YFP fluorophores was calculated using the Förster equation (*21*, *22*), where $R = R_o(1/E - 1)^{1/6}$. The Förster distance, R_o, was calculated as $R_o = (8.8 \times 10^{-23})(Q_D\kappa^2 n^{-4} J)^{1/6}$, where J is the overlap integral between CFP and YFP attached to the S1 expressed in M^{-1} cm^3 ($J = 2.18 \times 10^{-13}$), κ^2 is the orientation factor (assumed to be 0.667), n is the refractive index (assumed to be 1.4), and Q_D is the quantum yield (0.4 for CFP) obtained from the manufacturer's manual (Clontech). The calculated R_o was 4.86 nm.

In Vitro Motility Assay. A motility assay was performed as described previously (*17*). Briefly, after the RLC was phosphorylated by myosin light chain kinase, myc-tagged HMMs were allowed to bind to the nitrocellulose-coated glass surface of the flow cell by using a monoclonal antibody against c-myc (9E10, Pharmingen, San Diego, CA); 8 μL of the concentrated antibody solution (0.3 mg/mL) was used to create a dense HMM surface, and 8 μL of the diluted solution (0.075 mg/mL) was used to create a sparse HMM surface. Actin filaments labeled with rhodamine phalloidin were infused into the flow cell, and the sliding movement of actin filaments in the presence of ATP was observed using an epifluorescence inverted IX70 microscope (Olympus, Tokyo, Japan) equipped with a rhodamine filter set.

Optical Tweezers and Nanometry. We used an inverted fluorescence IX71 microscope (Olympus) equipped with optical tweezers (Sigma Koki, Tokyo, Japan) and a quadrant photodetector (Sentech, Osaka, Japan) (*23*, *24*). Optical tweezers were used to independently control two polystyrene beads. Experiments were performed in a flow cell made from two parallel coverslips. Polystyrene beads (2 μm) were decorated sparsely with myc-tagged phosphorylated HMMs using anti-c-myc antibody. The beads were allowed to bind to the nitrocellulose-coated coverslip surface in a solution containing 25 mM KCl, 5 mM $MgCl_2$, and 20 mM HEPES (pH 7.8). The solution was replaced with one containing rhodamine phalloidin-labeled actin filaments and 1 μm polystyrene beads that had been precoated with α-actinin. A single actin filament was attached at either end to a bead held in the optical tweezers. Interactions between actin and the surface-bound HMM were monitored by projecting the image of one of the beads onto the center of a quadrant photodetector after enlarging it 10^3 times. In the assay, the solution was supplemented with 1−10 μM ATP, 0.5% (v/v) 2-mercaptoethanol, and an oxygen-scavenger system (glucose oxidase, catalase, and glucose). The stiffness of the laser trap was calculated from the variance of the Brownian motion of the trapped bead, using the equipartition law, $^1/_2K\langle X^2\rangle = {}^1/_2K_bT$, where K is stiffness, $\langle X^2\rangle$ is the standard deviation of the bead position, K_b is Boltzmann's constant, and T is temperature.

RESULTS

Mutations Do Not Significantly Affect the Early or Late States of ATP Hydrolysis. The question of whether a perturbation affects the very early stages of the myosin process is best answered by comparing the performance of a mutated system with the wild-type system, focusing on the early rate constants that characterize each system. The

Table 1: Rate Constants and Extents of Interaction with Nucleotides and Actin in Wild-Type and Mutant HMMs

	parameter	wild type	F721A	F775A
mant-ATP binding[a]	increase (%)	100	104	104
	K_1k_2 (s^{-1} M^{-1})	3.3×10^5	3.3×10^5	3.2×10^5
Trp fluorescence[a]	increase (%)	18	14	13
	K_1k_2 (s^{-1} M^{-1})	2.7×10^5	1.9×10^5	2.1×10^5
	k_{max} (s^{-1})	230	large	130
	$K_{0.5}$ (mM)	1	large	0.7
mant-ADP release[a]	k_5 (s^{-1})	1.3	1.5	1
basic ATPase[b]	k_{cat} (s^{-1})	0.023 ± 0.001	0.058 ± 0.010	0.043 ± 0.001
actin-activated ATPase[c]	V_{max} (s^{-1})	2.1 ± 0.3	0.71 ± 0.02	2.0 ± 0.1
	K_{actin} (mM)	0.050 ± 0.012	0.043 ± 0.004	0.053 ± 0.007

[a] Conditions: 0.45 M KCl, 2 mM $MgCl_2$, and 20 mM Tris-HCl (pH 7.5) at 20 °C. [b] Conditions: 0.45 M KCl, 2 mM $MgCl_2$, and 20 mM Tris-HCl (pH 7.5) at 25 °C. [c] Conditions: 0.01 M KCl, 2 mM $MgCl_2$, and 20 mM Tris-HCl (pH 7.5) at 25 °C.

constants are given as k_i, k_{-i}, and K_i ($i = 1, 2, ...$) in the B−T chemical kinetic scheme (*10, 11*) (Scheme 1[2]).

Scheme 1

$$M + ATP \underset{k_{-1}}{\overset{k_1}{\rightleftarrows}} M\cdot ATP \underset{k_{-2}}{\overset{k_2}{\rightleftarrows}} M^*\cdot ATP \underset{k_{-3}}{\overset{k_3}{\rightleftarrows}} M^{**}\cdot ADP\cdot P_i \underset{k_{-4}}{\overset{k_4}{\rightleftarrows}} M^*\cdot ADP \underset{k_{-5}}{\overset{k_5}{\rightleftarrows}} M + ADP$$

The constants for the first process were experimentally measured using 2′(3′)-*O*-(*N*-methylanthraniloyl)adenosine 5′-triphosphate (mant-ATP) (*25*) in place of ATP so that the occupation of the active site can be inferred from the fluorescence emitted by the bound mant-ATP. Using mutant systems, addition of excess mant-ATP produced essentially the same increases in fluorescence that the wild-type system did (Table 1). The second-order rate constants (K_1k_2), estimated from the slope of the plots of the observed rate constant (k_{obs}) versus mant-ATP concentration, were very similar in the wild-type and mutant systems (Table 1). The second process, which was the conversion of M·ATP to M*·ATP, was measured directly in the three systems using the fact that Trp-512, located at the distal tip of the relay helix within the motor domain (*6*), enhances its fluorescence when the influence traveling from the active site reaches the helix (*15*, *26*, *27*). Upon addition of excess ATP, the increase in the Trp fluorescence for the mutant systems was only slightly smaller than that in the wild-type system (Table 1). Time transients of the fluorescence increase could be well fitted by a single exponential. The k_{obs} values were linearly dependent on ATP concentration at low ATP concentrations. The K_1k_2 values for the mutant systems were similar to those estimated from the development of mant fluorescence and close to the K_1k_2 value obtained for the wild-type system (Table 1).

However, the k_{obs} values were no longer linearly dependent on ATP concentration at greater ATP concentrations, in which range the dependence became quasi-hyperbolic [$k_{obs} \simeq k_{max}[ATP]/([ATP] + K_{0.5})$]. In the wild-type system, it is known that k_{max} corresponds to the rate of the hydrolytic transition (process 3 in the B−T sequence) (*28*). In the F775A system, the values of both k_{max} and $K_{0.5}$ were similar to those of the wild-type system; however, these parameters were too large to be measured in the F721A system (Table 1). It will be shown later that the mechanical linkage between the SH1 helix and the converter is completely disrupted in the F721A system. Normally, the acceleration of movement of the relay helix is slowed by the mass of the lever arm linked to the relay helix via the converter. We therefore may speculate that the large value of $k_3 + k_{-3}$ for the F721A system is the result of the faster movement of its relay helix, which is unregulated by the mass of the converter−lever arm system. We conclude that neither of our two perturbations significantly affects the events leading up to the arrival of the influence at the converter.

We also investigated whether the perturbations affected the two slow transitions (processes 4 and 5 in the B−T sequence) by measuring in each of the three systems the steady-state ATPase activity, and the rate of displacement of mant-ADP from the HMM·mant-ADP complex with excess ATP. The ATPase activities (k_{cat}) and the displacement rates (k_5) were similar in all three systems (Table 1). Moreover, it is interesting to note that the mutated systems exhibit actin activation (V_{max}) similar to that of the wild-type system (although F721A shows slightly lower levels), and that the K_{actin} values are also similar (Table 1). Together, the foregoing results show that the perturbations to be described next are specific effects produced on the converter, and not on any other element in the sequence.

Mutations Affect Movements of the Converter and the Lever Arm. For the first performance test of whether the mutations affect the lever arm movement, we constructed a test device, a chimeric S1[3] (C/Y-S1) in which YFP is fused to the N-terminus of the S1 heavy chain and CFP is fused to the N-terminus of the ELC. Because the CFP-to-YFP energy transfer between these fluorophores is well-understood and depends selectively on the distance between them, it is possible to detect their separation using optical measurements alone (*21*, *29*). Excitation of CFP at 433 nm resulted in a cyan emission at 450−515 nm, and the fluorescence energy transfer resulted in a yellow emission at 515−600 nm. When ATP or ADP was added to the wild-type C/Y-S1, the cyan emission from CFP decreased while the yellow emission from YFP increased (Figure 1A). The distance between the fluorophores decreased from 7.4 to 6.2 nm upon addition of ATP, and to 6.9 nm upon addition of ADP (Table 2). The distance between the termini, which was estimated

[2] In chemical notation, M stands for the truncated double-headed myosin that was used in our experiments, which is usually called HMM. Conformers of this protein, which can be distinguished by their absorbance or fluorescence, are denoted with one or two asterisks. As usual, k_i and k_{-i} are the forward and reverse rate constants, respectively of the *i*th reaction.

[3] To simplify the system, the single head of myosin, which is called S1, was used in this experiment.

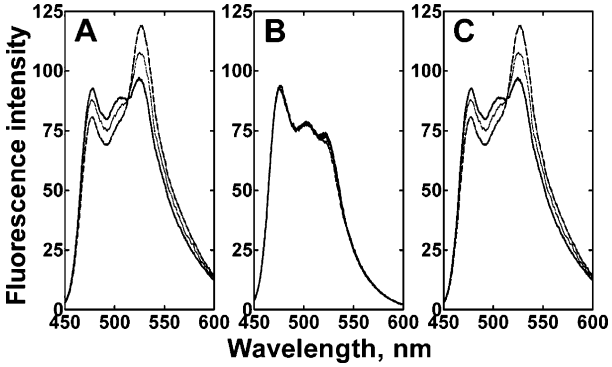

FIGURE 1: Fluorescence resonance energy transfer emission spectra. Emission spectra of wild-type (A), F721A (B), and F775A (C) C/Y-S1s excited at 433 nm were obtained in the absence of nucleotide (—), in the presence of 1 mM ATP (– – –), or in the presence of 0.1 mM ADP (•••). Conditions: 0.1 μM C/Y-S1s, 0.45 M KCl, 2 mM $MgCl_2$, 50 mM Tris-HCl (pH 8.0), and 0.5 mM dithiothreitol at 25 °C.

Table 2: Distances between CFP and YFP in Wild-Type and Mutant C/Y-S1s

C/Y-S1	nucleotide	FRET efficiency	distance (nm)
wild type	none	0.079 ± 0.010	7.4 ± 0.2
	ATP	0.183 ± 0.012	6.2 ± 0.1
	ADP	0.107 ± 0.008	6.9 ± 0.1
F721A	none	0.070 ± 0.005	7.3 ± 0.1
	ATP	0.082 ± 0.007	7.4 ± 0.1
	ADP	0.079 ± 0.001	7.4 ± 0.1
F775A	none	0.087 ± 0.002	7.5 ± 0.1
	ATP	0.201 ± 0.014	6.1 ± 0.1
	ADP	0.114 ± 0.024	6.9 ± 0.4

from the crystal structure of the motor domain complexed with an ATP analogue, was ~1.0 nm shorter than that estimated on the unligated motor domain (*3*, *7*). Therefore, the movement observed using the CFP fluorophore correlates well with the movement of the lever arm. When either ATP or ADP was added to the F721A C/Y-S1, there was no change in the energy transfer between the fluorophores (Figure 1B and Table 2). However, when these additions were made to the F775A C/Y-S1, the energy transfer changed just as it did in the wild-type C/Y-S1 (Figure 1C and Table 2). These results indicate that when either the wild-type or the F775A system undergoes the transition from the M to the M** state (see Scheme 1), it swings its lever arm, whereas the F721A system does not.

While the previous test examined the movement that myosin uses in carrying out its functions, the next two sample what is presumably the teleological function of myosin. We tested the speed at which actin is propelled [using a motility assay (*30*, *31*)], modulating the test severity by varying the resistance offered to its movement. On a surface that was densely covered with HMM molecules, the wild-type system propelled actin filaments at a speed of 0.51 ± 0.05 μm/s, but neither of the mutant systems moved actin filaments at all (Figure 2A). On a sparsely covered surface, the F721A system remained unable to propel actin filaments (Figure 2B). Surprisingly, however, we detected a slow movement of filaments by the F775A system (average velocity of 0.07 μm/s) under these conditions (Figure 2B). This indicates that although the F775A mutant retains the ability to swing its lever arm, its motor function is very weak. Mixing equal amounts of either F721A or F775A and the wild-type system

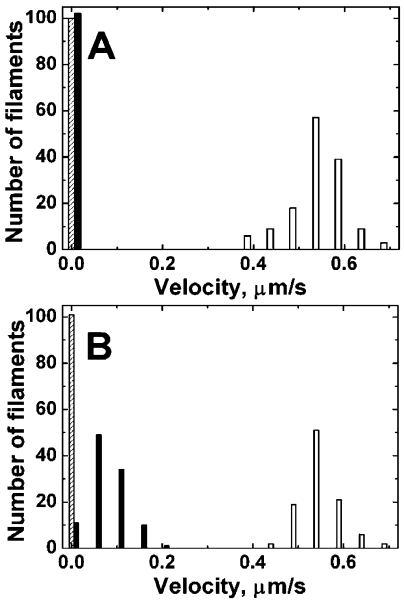

FIGURE 2: Distributions of the velocity of movement of actin filaments on glass surfaces densely (A) and sparsely (B) coated with HMMs: wild-type (empty), F721A (hatched), and F775A (filled). Conditions: 25 mM KCl, 3 mM $MgCl_2$, 20 mM HEPES (pH 7.8), and 2 mM ATP at 30 °C.

did not decrease the contribution of the wild-type component, indicating that the reduced motility expresses an inability of the mutant to generate force, but not irreversible binding of mutant dead heads to the actin filaments (data not shown).

In a final test of the wild-type and two mutated systems, we studied directly the ability of individual HMM molecules to exert force on actin. A single actin filament that was held taut by optical tweezers was brought close to a static bead that was sparsely coated with HMM molecules, and its position in space was sensitively monitored by projecting the bright-field image of the bead attached to the end of the actin filament onto a quadrant photodiode (*23*, *24*). Using weak trapping forces, there was significant thermal motion, which was expressed as positional variance of the held bead, except when actin—HMM interactions occurred. The equilibrium position without interactions between actin and HMM was defined as zero displacement. Both the wild-type and mutant systems showed periods of such low variance (therefore high stiffness) in their records (Figure 3A—F). The distribution of bead positions during these periods was fitted to a Gaussian curve, and the shift of the curve peak from the zero displacement position was called the size of the power stroke (Figure 3G—L). Under moderate trapping forces (stiffness of 0.03 pN/nm per bead), the shifts for both mutant systems were nearly zero (Figure 3I,K), which was much less than that of the wild-type system (6.5 ± 0.6 nm, Figure 3G). This indicates that neither of the mutants exerted sufficient force to pull the bead after the interaction between actin and HMM occurred. Next, we attempted to detect the weaker forces by lowering the stiffness of each trap to 0.008 pN/nm per bead. Under these conditions, the F775A system was able to pull the bead, although its power stroke was somewhat smaller than that of the wild-type system (5.5 and 6.9 nm, respectively; panels L and H of Figure 3). However, the F721A system was still unable to displace the bead under these conditions, even when so weakly trapped (Figure 3J). Thus, the results of this direct measurement of force correlate

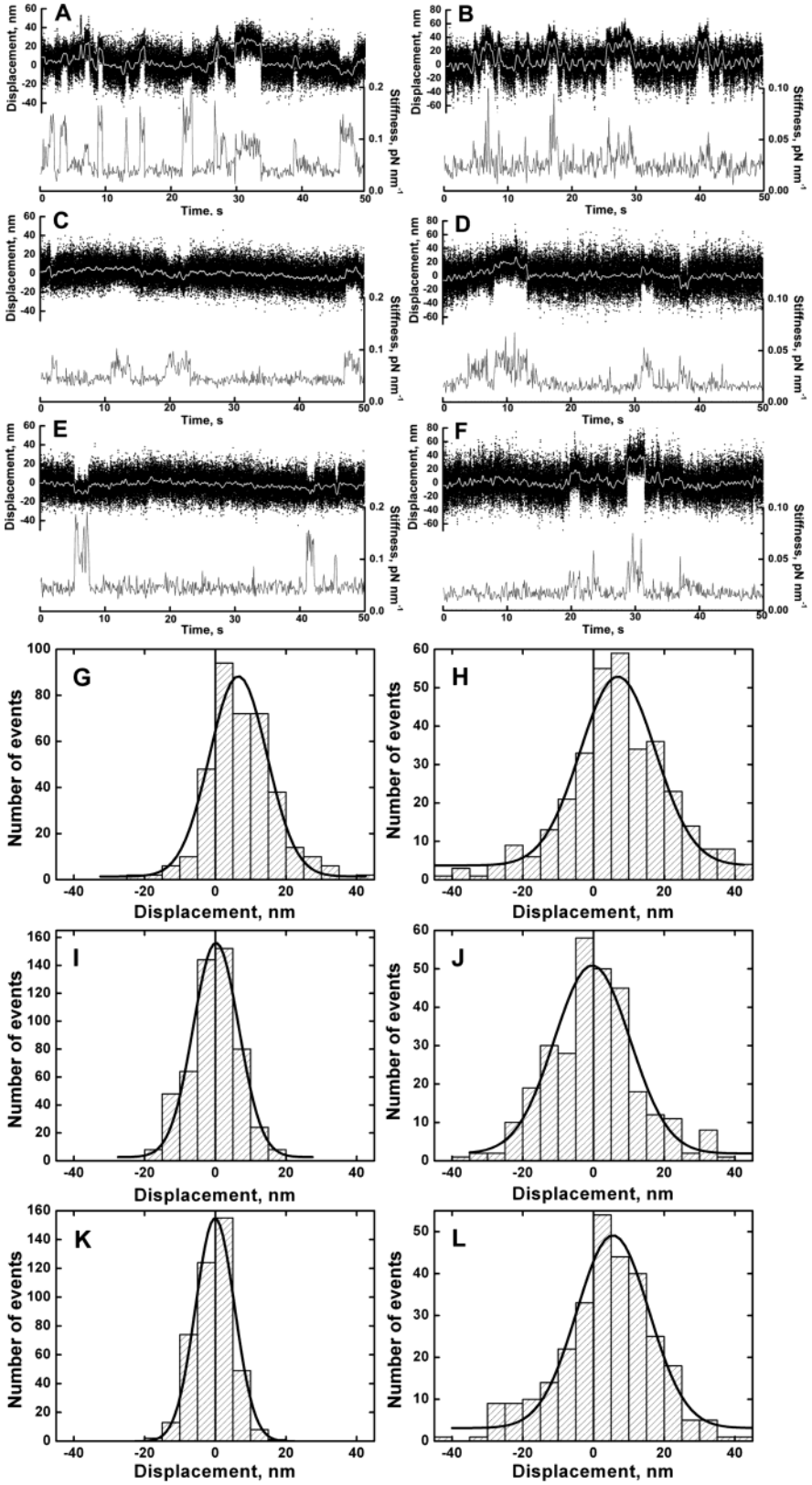

FIGURE 3: Displacements of actin filaments under moderately and extremely weak trapping forces caused by interactions with a single molecule of HMM. (A−F) In the data traces, the top traces show typical records of the displacements made by an HMM molecule at 1 μM ATP, the dots are raw data, the white lines are data passed through a low pass filter with a bandwidth of 2 Hz, and the bottom traces show stiffness calculated at intervals of 50 ms from the variance of the trapped bead position. (G−L) In the histograms of the displacements, solid vertical lines show the equilibrium (zero) position of the bead without interactions between actin and HMM. The fits to single Gaussian distributions are shown as solid lines. Mean sizes of the power stroke are 6.5 ± 0.6 nm for panel G, 6.9 ± 0.7 nm for panel H, 0.2 ± 0.4 nm for panel I, −0.4 ± 0.5 nm for panel J, −0.1 ± 0.4 nm for panel K, and 5.5 ± 0.7 nm for panel L. The trapping stiffness of each bead was 0.03 pN/nm for a moderately weak trapping force (A, C, E, G, I, and K) and 0.008 pN/nm for an extremely weak trapping force (B, D, F, H, J, and L). HMMs: wild-type (A, B, G, and H), F721A (C, D, I, and J), and F775A (E, F, K, and L). Conditions: 25 mM KCl, 5 mM $MgCl_2$, 20 mM HEPES (pH 7.8), and 1−10 μM ATP at ∼20 °C.

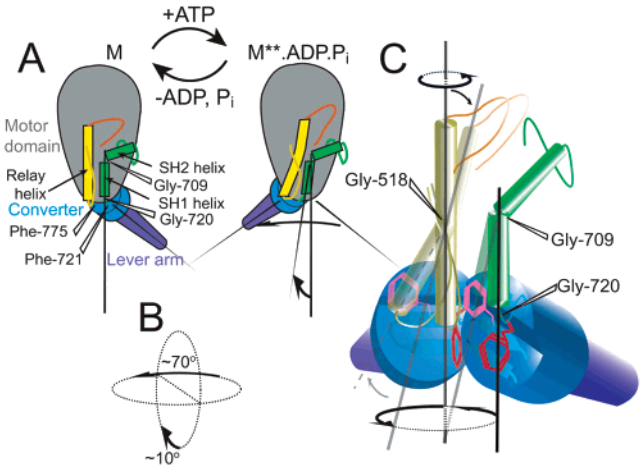

FIGURE 4: Mechanism by which motions within the motor domain are converted into a large rotation of the converter. (A) Lever arm swing. Myosin, initially in the M state (left), binds and rapidly hydrolyzes ATP to assume the metastable M**·ADP·P_i state (right). The relay helix and the SH1 (lower)/SH2 (upper) helices are shown as yellow and green rectangles, respectively. The ends of the relay helix are connected to the switch II loop (orange) and the converter (blue). The locations of Gly-709 (the flexible joint between the SH1 and SH2 helices), Gly-720 (the putative center for the rotation of the converter), and the two mutated residues (Phe-721 and Phe-775) are also shown. (B) ATP-induced conformational change, consisting of two almost perpendicular rotations. (C) Superimposition of nucleotide-free (the opaque image) and nucleotide-ligated (the translucent image) states. The converter and the lever arm are colored blue and purple, respectively. The switch II loop is shown as an orange strand, the relay loop as a silver strand, and the relay helix as a silver rod, and the SH1 (lower) and SH2 (upper) helices are shown as green rods. Arrows indicate the directions of shifts and rotations of the relay and SH1 helices that are induced by the closure of the nucleotide-binding cleft. The side chains of Phe-721 and Phe-775 are shown as red and pink hexagons, respectively. The β-sheet structure in the converter is shown as light-blue plane ribbons. The crystal structures of the skeletal muscle myosin with no nucleotide [Protein Data Bank (PDB) entry 2MYS] (*3*) and smooth muscle myosin complexed with MgADP·AlF_4^- (PDB entry 1BR4) (*7*) were adapted for the nucleotide-free and nucleotide-ligated myosin heads, respectively.

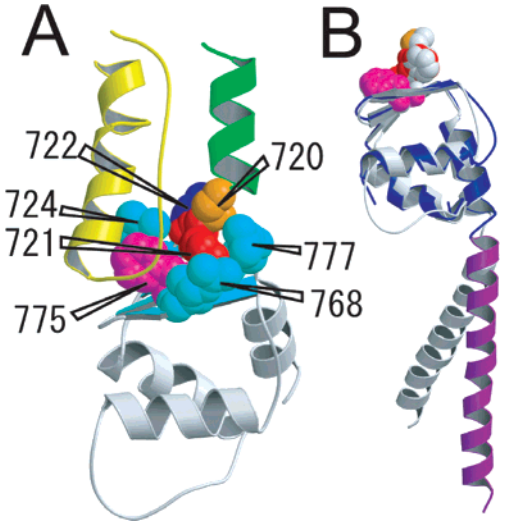

FIGURE 5: Structure and function of the small machine in the converter. (A) Enlarged view of the machine. The relay helix and loop are shown as a helical ribbon and a strand, respectively (both yellow). The SH1 helix is shown as a helical green ribbon. The three-stranded β-sheet is shown as plane ribbons (cyan), and all other structures in the converter are shown in white. Gly-720, Phe-721, Pro-722, Arg-724, Arg-768, Phe-775, and Arg-777 are presented as a CPK rendition. (B) Superposition of the converters in nucleotide-free and nucleotide-ligated myosin heads. In the former, the backbone atoms of the converter and a part of the lever arm are shown as blue and purple ribbons, respectively, and Gly-720 (orange), Phe-721 (red), and Phe-775 (pink) are presented as a CPK rendition. The latter is presented in the same manner, but all in white.

perfectly with those of the other performance tests (ability to swing the lever arm and to propel actin filaments in an *in vitro* motility assay), confirming that both mutations have special effects on the converter; the F775A mutation sharply inhibits its function but, unlike the F721A mutation, does not abolish it.

DISCUSSION

Since we can now refer to the three performance tests in Mutations Affect Movements of the Converter and the Lever Arm that report on the converter, we conclude that the two mutations had quite different effects on this element: the mutation at position 775 sharply inhibited its function, whereas the mutation at position 721 completely abolished it. We now describe the converter setting and its structure, and explain why these particular mutations were chosen. Thinking of the motor domain as fixed, we discuss the relative motion of the converter and the rigidly attached lever arm, focusing on the landmark of the SH1 helix (Figure 4A). The suggested movement of the converter when ATP is added to the distant active site is the sum of two almost perpendicular rotations: ~70° in the horizontal plane and ~10° in the vertical plane (*7*) (Figure 4B). These movements are enabled by the presence of Gly-720 (in the conserved Gly-Phe-Pro motif) at the helix−converter interface, and by Gly-709 of the helix (*7*). According to Rayment's studies of where crystal structures of the myosin head complexed with various ATP analogues belong in the catalytic cycle of ATP hydrolysis, the rotation of the converter domain occurs during the transition from the prehydrolysis state to the metastable state (ADP·P_i) after hydrolysis, or it occurs during the open-to-closed conformational change of the binding cleft (*5*, *6*, *32*, *33*).

The structure of the transmission system within the converter domain can be described in more detail as follows (Figure 5A). Three converter strands (residues 723−725, 766−770, and 773−777) form a β-sheet structure, and Phe-721 is in a compact hydrophobic cluster with Arg-768, Phe-775, and Arg-777 on the β-sheet. In the F721A system, the alanine substitute has no hydrophobic interaction with the cluster. The SH1 helix and the anterior part of the motor domain therefore lose contact with the converter stump and lever arm, which accounts for the uniform failure of this system in all of our tests of the lever arm swing and actin filament movements. In the F775A system, the normal hydrophobic interaction is absent, but Arg-724 and Arg-768 continue to form salt bridges with the relay helix; this might explain how the mutant continues to swing the lever arm and, albeit weakly, to move actin filaments. In normal operation, the side chain of Phe-775 is perpendicular to that of Phe-721, and makes direct contact with the distal end of the relay helix and the adjacent loop containing the ATP-sensitive Trp-512. These considerations suggest that, during the power stroke, the relay helix pushes the side chain of

Phe-775 with its tip, and rotates it around the principal axis of the SH1 helix.

We have further explored this speculation by comparing the structure of the relevant region (Gly-Phe-Pro motif and Phe-775) in its nucleotide-free and nucleotide-ligated states. The comparison reveals a largely unchanged structure, with the exception of a limited region in which a very small machine that accomplishes transmission seems to operate. The superimposition of images, as seen from the converter, reveals a rotation of ~70° around the principal axis of the SH1 helix in this area (Figure 4C and Movie S1 of the Supporting Information). Some movements are also observed near the relay helix and the SH1 helix. The rotation of this small machine is produced by the coordinated twisting motions of the two helices (circled arrows at the bottom), and further by the bending of the relay helix (translucent arrow). These motions of the transmission system can be created by the large Ramachandran angle changes at Gly-518 of the relay loop and at Gly-709 of the SH1 helix (*7*). The comparison between two converter structures in the nucleotide-free and nucleotide-ligated states revealed a high degree of similarity between states (Figure 5B), suggesting that the motion of the whole converter domain can largely be expressed as that of the little machine consisting of the Gly-Phe-Pro motif and Phe-775. Therefore, we suggest that this little machine is particularly important in positioning the converter−lever arm system. Other parts of the motor domain (for instance, the seven-stranded β-sheet structure core and the 25 kDa N-terminal domain) are also involved in the transmission of the force from the active site to the converter, but they seem to function as independent components of the overall motion.

Improved understanding of how the converter works gives a perspective of how overall transmission across myosin occurs. Closure of the cleft, which is induced by binding of the nucleotide to the active site, shifts the proximal end of the relay helix toward the active site (opaque arrow in Figure 4C), causing a clockwise rotation (as seen from the converter) (*5*, *34*). These movements cause a large rotation of the little machine consisting of two Phe residues linked to a Gly, through the cooperation of the relay helix, the relay loop, and the SH1 helix. Finally, this rotation is transmitted to the rigidly attached lever arm by the converter. *In situ*, the relay helix transmits mechanical changes in both the actin-detached and actin-attached states (during the reverse and power strokes, respectively) (*13*, *21*). However, under the circumstances that we describe, force is generated more effectively during the power stroke than during the reverse stroke. This is because the former occurs through a pushing motion of the side chain of Phe-775, whereas the latter occurs through a pulling motion, perhaps using hydrophobic interactions between the relay helix and the converter.

ACKNOWLEDGMENT

We thank K. Konishi for her early contribution to this study and T. Yanagida, H. Tanaka, and T. Watanabe for helping us assemble a microscope equipped with laser tweezers and a quadrant photodetector. We also thank T. J. Pearson for significant improvements to our manuscript.

SUPPORTING INFORMATION AVAILABLE

Movie showing a schematic three-dimensional model of the actions of the transmission machinery of myosin. This material is available free of charge via the Internet at http://pubs.acs.org.

REFERENCES

1. Huxley, H. E. (1969) The mechanism of muscular contraction, *Science 164*, 1356−1365.
2. Huxley, A. F., and Simmons, R. M. (1971) Proposed mechanism of force generation in striated muscle, *Nature 233*, 533−538.
3. Rayment, I., Rypniewski, W. R., Schmidt-Bäse, K., Smith, R., Tomchick, D. R., Benning, M. M., Winkelmann, D. A., Wesenberg, G., and Holden, H. M. (1993) Three-dimensional structure of myosin subfragment-1: a molecular motor, *Science 261*, 50−58.
4. Rayment, I., Holden, H. M., Whittaker, M., Yohn, C. B., Lorenz, M., Holmes, K. C., and Milligan, R. A. (1993) Structure of the actin-myosin complex and its implications for muscle contraction, *Science 261*, 58−65.
5. Fisher, A. J., Smith, C. A., Thoden, J. B., Smith, R., Sutoh, K., Holden, H. M., and Rayment, I. (1995) X-ray structures of the myosin motor domain of *Dictyostelium discoideum* complexed with MgADP·BeF_x and MgADP·AlF_4^-, *Biochemistry 34*, 8960−8972.
6. Smith, C. A., and Rayment, I. (1996) X-ray structure of the magnesium(II)·ADP·vanadate complex of the *Dictyostelium discoideum* myosin motor domain to 1.9 Å resolution, *Biochemistry 35*, 5404−5417.
7. Dominguez, R., Freyzon, Y., Trybus, K. M., and Cohen, C. (1998) Crystal structure of a vertebrate smooth muscle myosin motor domain and its complex with the essential light chain: visualization of the pre-power stroke state, *Cell 94*, 559−571.
8. Houdusse, A., Szent-Györgyi, A. G., and Cohen, C. (2000) Three conformational states of scallop myosin S1, *Proc. Natl. Acad. Sci. U.S.A. 97*, 11238−11243.
9. Holmes, K. C., Angert, I., Kull, F. J., Jahn, W., and Schröder, R. R. (2003) Electron cryo-microscopy shows how strong binding of myosin to actin releases nucleotide, *Nature 425*, 423−427.
10. Bagshaw, C. R., and Trentham, D. R. (1974) The characterization of myosin-product complexes and of product-release steps during the magnesium ion-dependent adenosine triphosphatase reaction, *Biochem. J. 141*, 331−349.
11. Bagshaw, C. R., Eccleston, J. F., Eckstein, F., Goody, R. S., Gutfreund, H., and Trentham, D. R. (1974) The magnesium ion-dependent adenosine triphosphatase of myosin. Two-step processes of adenosine triphosphate association and adenosine diphosphate dissociation, *Biochem. J. 141*, 351−364.
12. Onishi, H., Ohki, T., Mochizuki, N., and Morales, M. F. (2002) Early stages of energy transduction by myosin: roles of Arg in switch I, of Glu in switch II, and of the salt-bridge between them, *Proc. Natl. Acad. Sci. U.S.A. 99*, 15339−15344.
13. Onishi, H., Mochizuki, N., and Morales, M. F. (2004) On the myosin catalysis of ATP hydrolysis, *Biochemistry 43*, 3757−3763.
14. Malnasi-Csizmadia, A., Woolley, R. J., and Bagshaw, C. R. (2000) Resolution of conformational states of *Dictyostelium* myosin II motor domain using tryptophan (W501) mutants: implications for the open-closed transition identified by crystallography, *Biochemistry 39*, 16135−16146.
15. Malnasi-Csizmadia, A., Kovacs, M., Woolley, R. J., Botchway, S. W., and Bagshaw, C. R. (2001) The dynamics of the relay loop tryptophan residue in the *Dictyostelium* myosin motor domain and the origin of spectroscopic signals, *J. Biol. Chem. 276*, 19483−19490.
16. Yanagisawa, M., Hamada, Y., Katsuragawa, Y., Imamura, M., Mikawa, T., and Masaki, T. (1987) Complete primary structure of vertebrate smooth muscle myosin heavy chain deduced from its complementary DNA sequence. Implications on topography and function of myosin, *J. Mol. Biol. 198*, 143−157.
17. Kojima, S., Fujiwara, K., and Onishi, H. (1999) SH1 (cysteine 717) of smooth muscle myosin: its role in motor function, *Biochemistry 38*, 11670−11676.
18. Kunkel, T. A., Roberts, J. D., and Zakour, R. A. (1987) Rapid and efficient site-specific mutagenesis without phenotypic selection, *Methods Enzymol. 154*, 367−382.

19. Konishi, K., Kojima, S., Katoh, T., Yazawa, M., Kato, K., Fujiwara, K., and Onishi, H. (2001) Two new modes of smooth muscle myosin regulation by the interaction between the two regulatory light chains, and by the S2 domain, *J. Biochem. 129*, 365−372.
20. Onishi, H., Maéda, K., Maéda, Y., Inoue, A., and Fujiwara, K. (1995) Functional chicken gizzard heavy meromyosin expression in and purification from baculovirus-infected insect cells, *Proc. Natl. Acad. Sci. U.S.A. 92*, 704−708.
21. Suzuki, Y., Yasunaga, T., Ohkura, R., Wakabayashi, T., and Sutoh, K. (1998) Swing of the lever arm of a myosin motor at the isomerization and phosphate-release steps, *Nature 396*, 380−383.
22. Stryer, L. (1978) Fluorescence energy transfer as a spectroscopic ruler, *Annu. Rev. Biochem. 47*, 819−846.
23. Finer, J. T., Simmons, R. M., and Spudich, J. A. (1994) Single myosin molecule mechanics: piconewton forces and nanometre steps, *Nature 368*, 113−119.
24. Molloy, J. E., Burns, J. E., Kendrick-Jones, J., Tregear, R. T., and White, D. C. (1995) Movement and force produced by a single myosin head, *Nature 378*, 209−212.
25. Hiratsuka, T. (1983) New ribose-modified fluorescent analogs of adenine and guanine nucleotides available as substrates for various enzymes, *Biochim. Biophys. Acta 742*, 496−508.
26. Batra, R., and Manstein, D. J. (1999) Functional characterization of *Dictyostelium* myosin II with conserved tryptophanyl residue 501 mutated to tyrosine, *Biol. Chem. 380*, 1017−1023.
27. Onishi, H., Konishi, K., Fujiwara, K., Hayakawa, K., Tanokura, M., Martinez, H. M., and Morales, M. F. (2000) On the tryptophan residue of smooth muscle myosin that responds to binding of nucleotide, *Proc. Natl. Acad. Sci. U.S.A. 97*, 11203−11208.
28. Marston, S. B., and Taylor, E. W. (1980) Comparison of the myosin and actomyosin ATPase mechanisms of the four types of vertebrate muscles, *J. Mol. Biol. 139*, 573−600.
29. Majoul, I., Straub, M., Duden, R., Hell, S. W., and Soling, H. D. (2002) Fluorescence resonance energy transfer analysis of protein−protein interactions in single living cells by multifocal multiphoton microscopy, *J. Biotechnol. 82*, 267−277.
30. Harada, Y., Noguchi, A., Kishino, A., and Yanagida, T. (1987) Sliding movement of single actin filaments on one-headed myosin filaments, *Nature 326*, 805−808.
31. Kron, S. J., and Spudich, J. A. (1986) Fluorescent actin filaments move on myosin fixed to a glass surface, *Proc. Natl. Acad. Sci. U.S.A. 83*, 6272−6276.
32. Gulick, A. M., Bauer, C. B., Thoden, J. B., and Rayment, I. (1997) X-ray structures of the MgADP, MgATPγS, and MgAMPPNP complexes of the *Dictyostelium discoideum* myosin motor domain, *Biochemistry 36*, 11619−11628.
33. Bauer, C. B., Holden, H. M., Thoden, J. B., Smith, R., and Rayment, I. (2000) X-ray structures of the apo and MgATP-bound states of *Dictyostelium discoideum* myosin motor domain, *J. Biol. Chem. 275*, 38494−38499.
34. Fisher, A. J., Smith, C. A., Thoden, J., Smith, R., Sutoh, K., Holden, H. M., and Rayment, I. (1995) Structural studies of myosin:nucleotide complexes: a revised model for the molecular basis of muscle contraction, *Biophys. J. 68*, 19S−26S.

BI048954F